Louisiana State University
LSU Digital Commons

LSU Master's Theses | Graduate School

2015

An Analytic Solution of the Thermal Boundary Layer at the Leading Edge of a Heated Semi-Infinite Flat Plate under Forced Uniform Flow

Robert Jessee
Louisiana State University and Agricultural and Mechanical College, rjesse1@tigers.lsu.edu

Follow this and additional works at: https://digitalcommons.lsu.edu/gradschool_theses

 Part of the Mechanical Engineering Commons

Recommended Citation
Jessee, Robert, "An Analytic Solution of the Thermal Boundary Layer at the Leading Edge of a Heated Semi-Infinite Flat Plate under Forced Uniform Flow" (2015). *LSU Master's Theses*. 2013.
https://digitalcommons.lsu.edu/gradschool_theses/2013

This Thesis is brought to you for free and open access by the Graduate School at LSU Digital Commons. It has been accepted for inclusion in LSU Master's Theses by an authorized graduate school editor of LSU Digital Commons. For more information, please contact gradetd@lsu.edu.

AN ANALYTIC SOLUTION OF THE THERMAL BOUNDARY LAYER AT THE LEADING EDGE OF A HEATED SEMI-INFINITE FLAT PLATE UNDER FORCED UNIFORM FLOW

A Thesis

Submitted to the Graduate Faculty of the
Louisiana State University and
Agricultural and Mechanical College
in partial fulfillment of the
requirements for the degree of
Master of Science in Mechanical Engineering

in

The Department of Mechanical and Industrial Engineering

by
Robert Lawrence Jessee
B.S., Clemson University, 2008
December 2015

Acknowledgements

I would like to first acknowledge and express my gratitude for my friend and colleague, Mr. Sai Sashankh Rao, who was the first to develop a solution to the fluid portion of this problem. His methodology and insight were of great assistance, and it was a privilege to work alongside him during all stages of my research.

I would also like to thank my advisor, Dr. Harris Wong, whose patience and keen intellect were instrumental in both the development of this work and in the growth and expansion of my own understanding. I am indebted to him for his time spent in guiding and teaching me, and am very thankful to have been able to study under and learn from him.

I would like to recognize the Louisiana State University Department of Mechanical Engineering for their support over the last two years. Without their financial assistance I would not have been able to continue this work, and I am grateful for the opportunities given to me by their generosity and support.

Statement of Originality

The following thesis contains no material which has been accepted for the award of any other degree or diploma in any university or other tertiary institution, and to the best of my knowledge, contains no material previously published or written by another person, except where due reference has been made.

Robert Lawrence Jessee, December 2015

Table of Contents

Abstract

The heated flat plate under uniform flow has been vastly studied, with the Blasius and Pohlhausen solutions developed over 100 years ago. These solutions are numerical in nature. Here, an analytic solution is found for the temperature and velocity profiles at the leading edge of a heated flat plate under forced uniform flow. By defining a similarity variable the governing equations are reduced to a dimensionless equation with an analytic solution at the leading edge. This report gives justification for the similarity variable via scaling analysis, details the process of converting to similarity form, and presents a similarity solution. The analytic fluid and thermal solutions are then checked against a numerical solution obtained via computational dynamics.

1 Introduction

1.1 Literature Review

In 1904 Ludwig Prandtl changed fluid dynamics by publishing the paper "Über Flüssigkeitsbewegung bei sehr kleiner Reibung" ("On the Motion of Fluids with Very Little Friction"), in which he proposed the existence of a fluid boundary layer, defined as a thin region near a stationary surface in a moving fluid stream where shear stresses cannot be neglected [1, 2, 3]. This concept was studied by Prandtl and his students, eventually resulting in Heinrich Blasius producing his classic paper in 1908 wherein he derived the fluid profile for 2D boundary-layer flow over both a flat plate with no pressure gradient and over a circular cylinder [4]. Thirteen years later, E. Pohlhausen used the Blasius boundary layer solution to solve for the thermal boundary layer over the flat plate, completing the boundary layer profile for the flat plate by coupling the fluid and thermal solutions [5].

The following years saw large strides in the studying and understanding of boundary-layer flows. Since boundary-layer solutions provide information about drag and heat transfer at the surface of an object in a fluid stream, the solutions to these boundary layers allow for the calculation of drag and lift forces, as well as heat transfer from the solid surface. Thermal boundary layers are typically classified according to the velocity field into either forced or natural flows. Forced-flow boundary layers are due to an imposed velocity field, while natural-flow boundary layers are due to velocity gradients that arise from buoyant forces. During the 20th century boundary layers were analyzed with great mathematic rigor, resulting in multiple additions to the Blasius flat-plate solution as well as in the description of the boundary layers of other geometries.

In the same year that Pohlhausen developed his thermal boundary layer, von Karman developed a method for calculating the boundary-layer thickness. This von Karmen boundary-layer momentum integral equation has been shown to be valid for both laminar boundary layers and turbulent, time-averaged boundary layers, and is still studied in fluid mechanics and heat transfer courses today [6]. In 1931 Falkner and Skan developed similarity solutions for boundary layers with more general conditions than that developed by Blasius, one of which was the flat plate without a negligible pressure gradient [7]. In the late 1940's, Thwaites built on the work of Holstein and Bohlen to develop an approximate solution to the von Karman equation, providing a better description of the flat plate laminar-boundary-layer [6, 8].

These solutions were only the beginning to the research analyzing the flat plate. In 1961 Ting modified the boundary layer equations to describe the flat plate in the presence of a shear flow, resulting in a similarity solution to the boundary layer when the vorticity number is large [9]. Ting's work was built upon by Devan in 1965, wherein he developed an approximate numerical solution to Ting's boundary layer in the presence of shear flow, utilizing a perturbation expansion in the Reynolds number to obtain his governing equations

[10].

Because of its simplicity the flat plate has been studied for both incompressible and compressible flow under laminar, transitional, and turbulent conditions. It has been analyzed with the plate stationary and with the plate impulsively-started, as well as with non-zero velocity at the surface. Mass diffusion has been characterized, as has a boundary-layer with unsteady chemical reactions taking place. The beauty of the plate lies in its simplicity, and it is this aspect of the problem that motivates this study of the boundary layer located at the leading edge.

1.2 Scope

The primary objective of this work is to obtain a more complete picture of the flat plate thermal boundary-layer by developing a solution that is valid at the leading edge. While of limited practical applications, this approach presents a useful theoretical exercise that could lead to similar-type solutions in other boundary layer flows, and the flat plate was a logical starting point due to its simplicity.

This work follows a similar approach to that of Blasius, in that an order-of-magnitude analysis is used to determine the correlation between variables where the problem imposes no physical scale. Once obtained, this scale is used to define a similarity variable and similarity functions that can be used to convert the governing partial differential equations (PDEs) into ordinary differential equations (ODEs). Additional simplifications are made based on the physics of the problem, and an analytic solution obtained.

In order to verify the accuracy of the analytic solution a numeric solution is obtained via a computational fluid dynamics (CFD) simulation using ANSYS FLUENT. The analytic solution is used to predict the thermal-boundary-layer profile of the flow, and the results are compared at Reynolds numbers from $0.001 \leq Re_x \leq 1.0$.

2 Theoretical Analysis

2.1 Problem Setup

Consider a heated flat plate at temperaure T_p, unbounded at one end, subjected to an imposed uniform flow of velocity U_∞ at temperature T_∞. A cartesian coordinate system is defined such that the origin is placed at the tip of the plate, with x increasing along the length of the plate and y increasing normal to the plate, as shown in Figure 1. The flow is considered to be laminar and incompressible with constant fluid properties.

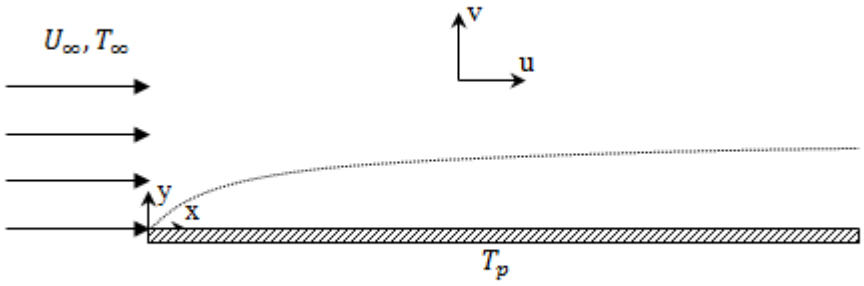

Figure 1: Heated semi-infinite flat plate under forced uniform flow.

The boundary-layer fluid flow is governed by the Navier-Stokes equations for a fluid with constant density and viscosity, given by Equations 1 - 3,

$$\frac{\partial u}{\partial x} + \frac{\partial v}{\partial y} = 0 \tag{1}$$

$$\rho\left(u\frac{\partial u}{\partial x} + v\frac{\partial u}{\partial y}\right) = -\frac{\partial p}{\partial x} + \mu\left(\frac{\partial^2 u}{\partial x^2} + \frac{\partial^2 u}{\partial y^2}\right) \tag{2}$$

$$\rho\left(u\frac{\partial v}{\partial x} + v\frac{\partial v}{\partial y}\right) = -\frac{\partial p}{\partial y} + \mu\left(\frac{\partial^2 v}{\partial x^2} + \frac{\partial^2 v}{\partial y^2}\right), \tag{3}$$

where ρ is the density of the fluid and μ is the dynamic viscosity. The thermal boundary-layer can be described using the steady-state, constant-property convection energy equation,

$$u\frac{\partial T}{\partial x} + v\frac{\partial T}{\partial y} = \alpha\left(\frac{\partial^2 T}{\partial x^2} + \frac{\partial^2 T}{\partial y^2}\right), \tag{4}$$

where α is the thermal diffusivity.

Boundary conditions can be obtained by enforcing the no-slip and constant-surface-temperature conditions at the plate. These are coupled with far-field conditions that, far away from the plate, the boundary-layer velocity and temperature approaches that of the forced flow. Additionally, the velocity and temperature of the boundary-layer at the tip of the plate is equal to that of the incoming flow. These boundary conditions are listed in Table 1.

Table 1: Boundary conditions for the fluid and thermal boundary-layers.

1. At $y = 0$, $u = 0$
2. At $y = 0$, $v = 0$
3. At $x = 0$, $u = U_\infty$
4. As $y \to \infty$, $u \to U_\infty$
5. As $y \to \infty$, $v \to 0$
6. At $y = 0$, $T = T_p$
7. As $y \to \infty$, $T \to T_\infty$

2.2 Similarity Conversion

2.2.1 Conversion to stream function

Because the flow is two-dimensional and incompressible, the number of dependent variables can be reduced from three to two through the use of the stream function, ψ, where u is defined as $\partial\psi/\partial y$ and v is defined as $-\partial\psi/\partial x$. Substituting the definition for the stream function into Equations 1 - 4, continuity is automatically satisfied and the momentum and energy equations are given in Equations 5 - 7.

$$\rho\left(\frac{\partial\psi}{\partial y}\frac{\partial^2\psi}{\partial x\partial y} - \frac{\partial\psi}{\partial x}\frac{\partial^2\psi}{\partial y^2}\right) = -\frac{\partial p}{\partial x} + \mu\left(\frac{\partial^3\psi}{\partial x^2\partial y} + \frac{\partial^3\psi}{\partial y^3}\right) \tag{5}$$

$$\rho\left(-\frac{\partial\psi}{\partial y}\frac{\partial^2\psi}{\partial x^2} + \frac{\partial\psi}{\partial x}\frac{\partial^2\psi}{\partial x\partial y}\right) = -\frac{\partial p}{\partial y} + \mu\left(-\frac{\partial^3\psi}{\partial x^3} - \frac{\partial^3\psi}{\partial x\partial y^2}\right) \tag{6}$$

$$\frac{\partial\psi}{\partial y}\frac{\partial T}{\partial x} - \frac{\partial\psi}{\partial x}\frac{\partial T}{\partial y} = \alpha\left(\frac{\partial^2 T}{\partial x^2} + \frac{\partial^2 T}{\partial y^2}\right) \tag{7}$$

Equations 5 and 6 can be cross-differentiated and subtracted in order to eliminate the pressure term, combining both momentum equations into a single equation while also eliminating an unknown variable.

Differentiating (5) with respect to y, (6) with respect to x, and taking the difference of the two yields a combined momenum equation, Equation 8.

$$\rho[\frac{\partial\psi}{\partial y}(\frac{\partial^3\psi}{\partial x\partial y^2}+\frac{\partial^3\psi}{\partial^3 x})-\frac{\partial\psi}{\partial x}(\frac{\partial^3\psi}{\partial x^2\partial y}+\frac{\partial^3\psi}{\partial^3 y})]=\mu[\frac{\partial^4\psi}{\partial x^4}+2\frac{\partial^4\psi}{\partial x^2\partial y^2}+\frac{\partial^4\psi}{\partial y^4}] \tag{8}$$

This is the governing equation for the fluid flow in terms of two independent variables, x and y, and one dependent variable, ψ.

2.2.2 Scaling and Similarity Transformation

Because the flat plate is unbounded in the positive x and y directions, a similarity variable can be defined that will allow for the reduction in the number of independent variables from two to one. In order to complete the similarity transformation, an order-of-magnitude analysis is required to determine the relation between the y and x scales. Each scale is defined in Table 2, and the scales are then used in conjunction with Equations 1 - 4 and the physical parameters of the problem to determine an appropriate relationship between scales.

Table 2: List of scaling parameters

$x \sim \delta x$	$y \sim \delta y$	$u \sim U_\infty$	$v \sim \delta v$	$T \sim \Delta T$	$\psi \sim U_\infty \delta y$

The symbol $\sim$ should be interpreted "is of the same order of magnitude as," and ΔT is defined as $\Delta T = T_p - T_\infty$. Substituing these definitions into (1) and rearranging, the x and y scales relate to the u and v scales according to (9).

$$\frac{U_\infty}{\delta x} \sim \frac{\delta v}{\delta y} \tag{9}$$

Close to the tip of the plate, viscous forces should dominate. Therefore, the nonlinear inertial terms in (8) should drop, and balance of the viscous terms yields

$$\delta y \sim \delta x. \tag{10}$$

The scales for the dependent variables ψ and T can be determined using the definition of ψ and the physical parameters, respectively.

This scale between y and x can be used to define a similarity variable, η, where η is defined as $\frac{y}{\delta y}$. Dimensionless similarity functions $f(\eta)$ and $\widehat{T}(\eta)$ may also be defined for T and ψ based on ΔT and $\delta\psi$, where $f(\eta) = \frac{\psi}{\delta\psi}$ and describes the fluid boundary-layer, and $\hat{T}(\eta) = \frac{T-T_\infty}{\Delta T}$ and describes the thermal

boundary-layer. From the scaling analysis, $\delta y \sim \delta x = x$, and $\delta\psi \sim \delta u \delta y = U_\infty x$. Using these definitions, the similarity tranformations are given below.

$$\eta = \frac{y}{x} \tag{11}$$

$$f(\eta) = \frac{\psi}{U_\infty x} \tag{12}$$

$$\widehat{T}(\eta) = \frac{T - T_\infty}{\Delta T} \tag{13}$$

Equations 11 - 13 can be substituted into the governing equations, 7 and 8. After appropriate differentiation and substitution of the similarity variable and functions, Equations 7 and 8 become

$$-Re_x[(\eta^2+1)f^{'''}f^{'} + (\eta^2+1)f^{''}f^{'} + 2\eta f^{''}f] = (\eta^2+1)^2 f^{(4)} + 8\eta(\eta^2+1)f^{'''} + 4(3\eta^2+1)f^{''} \tag{14}$$

$$(\eta^2+1)\widehat{T}^{''}(\eta) + [2\eta + Re_x Pr f(\eta)]\widehat{T}^{'}(\eta) = 0 \tag{15}$$

where Re_x and Pr are the Reynolds number based on x and the Prandtl number, and are respectively defined below.

$$Re_x = \frac{U_\infty x}{\nu} \tag{16}$$

$$Pr = \frac{\nu}{\alpha} \tag{17}$$

The boundary conditions can be transformed into similarity form as well, and are given in Table 3. Note that boundary conditions 3 and 4 combine into a single similarity boundary condition, 3.

Table 3: Similarity boundary conditions for the fluid and thermal boundary-layers.

1. At $\eta = 0$, $f'(\eta) = 0$
2. At $\eta = 0$, $f(\eta) = 0$
3. As $\eta \to \infty$, $f'(\eta) \to 1$
4. As $\eta \to \infty$, $f(\eta) \to 0$
5. At $\eta = 0$, $\widehat{T} = 1$
6. As $\eta \to \infty$, $\widehat{T} \to 0$

2.3 Leading Order Solution

At the plate's leading edge viscous forces should dominate. This implies that the Reynolds number is much less than unity. Taking the limit as $Re_x \to 0$, (14) and (15) become

$$(\eta^2 + 1)^2 f^{(4)} + 8\eta(\eta^2 + 1) f^{'''} + 4(3\eta^2 + 1) f^{''} = 0 \tag{18}$$

$$(\eta^2 + 1)\widehat{T}^{''}(\eta) + 2\eta\widehat{T}(\eta) = 0, \tag{19}$$

provided that the Prandtl number is finite. Both equations can be solved analytically. The solution to (18) was first solved by S. S. Rao, and the solution to (19) is given below in Equation 21.

$$f(\eta) = \tfrac{1}{2}\tan^{-1}(\eta)\left[C_1\eta - C_2\right] + C_3\eta + C_4 \tag{20}$$

$$\widehat{T}(\eta) = C_5\tan^{-1}(\eta) + C_6 \tag{21}$$

Boundary condition 2 from Table 3 gives $C_4 = 0$, and condition 1 gives $C_2 = 2C_3$. Since boundary conditions 3 and 4 are imposed in the limit as η approaches infinity, determining the constants C_3 and C_1 requires that $\tan^{-1}(\eta)$ be expanded in an asymptotic series as $\eta \to \infty$. Performing the expansion and enforcing condition 3 gives $C_3 = 1 - \frac{\pi}{4}C_1$, and condition 4 gives $C_1 = \frac{4\pi}{\pi^2 - 4}$. Substituting these constants into Equation 20 gives the leading-order fluid solution, given in Equation 22.

$$f(\eta) = \frac{1}{\left(\frac{\pi}{2}\right)^2 - 1}\left[\left(\frac{\pi}{2}\eta - 1\right)\tan^{-1}(\eta) - \eta\right] \tag{22}$$

Boundary condition 5 from Table 3 gives that $C_6 = 1$. Since boundary condition 6 is enforced as $\eta \to \infty$,

determining C_5 requires that $tan^{-1}(\eta)$ be expanded in an asymptotic series as $\eta \to \infty$. Performing the expansion and taking the limit as $\eta \to \infty$ gives $C_5 = -\frac{2}{\pi}$. Substituting these constants into (21) gives the leading-order solution as

$$\widehat{T}(\eta) = 1 - \frac{2}{\pi}\tan^{-1}(\eta). \tag{23}$$

This solution is valid as long as the Reynolds number is low and the Prandtl number is finite.

3 Numeric Verification

In order to verify the accuracy of the analytic solution the solution can be tested using computation fluid dynamics (CFD) analysis or experimentation. One benefit to CFD verification over experimental verification is the ability to easily vary physical parameters to determine how well the analytic matches the numeric solution. Additionally, the small dimensions of the leading-edge portion of the flat plate boundary layer would present significant experimental difficulties, since a large degree of instrumental precision would be required to analyze the boundary layer flow at such small scales. These factors combined make numeric verification the better option.

3.1 Problem Non-Dimensionalization

When conducting numeric simulations the domain must be discretized to match the problem of interest. This discretization requires both an input value and a unit, but since nature is dimensionless the domain values should be used to normalize the governing equations so that the analysis can be manipulated in dimensionless form. In order to achieve this, consider the dimensional form of the governing equations and plate, given in Figure 2.

$$\rho\left(u\frac{\partial u}{\partial x}+v\frac{\partial u}{\partial y}\right)=-\frac{\partial p}{\partial x}+\mu\left(\frac{\partial^2 u}{\partial x^2}+\frac{\partial^2 u}{\partial y^2}\right) \tag{2}$$

$$\rho\left(u\frac{\partial v}{\partial x}+v\frac{\partial v}{\partial y}\right)=-\frac{\partial p}{\partial y}+\mu\left(\frac{\partial^2 v}{\partial x^2}+\frac{\partial^2 v}{\partial y^2}\right) \tag{3}$$

$$u\frac{\partial T}{\partial x}+v\frac{\partial T}{\partial y}=\alpha\left(\frac{\partial^2 T}{\partial x^2}+\frac{\partial^2 T}{\partial y^2}\right) \tag{4}$$

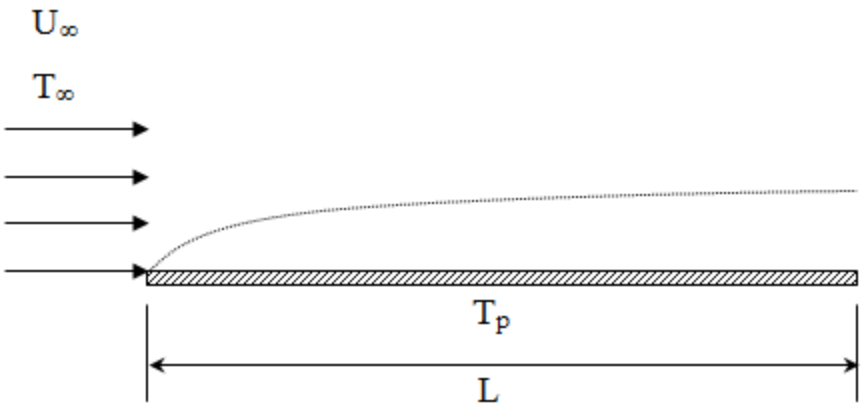

Figure 2: Dimensional problem setup for the flat plate.

Using the physical properties of the problem, dimensionless parameters are defined in Table 4.

Table 4: Dimensionless parameters for numerical simulation

$$x^* = \frac{x}{L} \qquad y^* = \frac{y}{L} \qquad u^* = \frac{u}{U_\infty} \qquad v^* = \frac{v}{U_\infty} \qquad p^* = \frac{p}{\mu U_\infty / L} \qquad T^* = \frac{T - T_\infty}{T_p - T_\infty}$$

The spatial variables x and y have been non-dimensionalized by the plate length L, and the velocity variables u and v by the free-stream velocity, U_∞. The pressure term has been balanced with the viscous rather than the inertial term since viscous forces are expected to dominate near the leading edge. Temperature is made non-dimensional by taking the ratio of the difference between the boundary-layer and free-stream temperature to the difference between the plate temperature and the free-stream temperature.

Substituting these definitions into Equations 2 - 4 and simplifying gives the dimensionless form of the governing equations in addition to non-dimensionalizing the domain. The non-dimensionalized problem is given below by Equations 24 - 26 and by Figure 3,

$$Re_L \left(u^* \frac{\partial u^*}{\partial x^*} + v^* \frac{\partial u^*}{\partial y^*} \right) = -\frac{\partial p^*}{\partial x^*} + \frac{\partial^2 u^*}{\partial x^{*2}} + \frac{\partial^2 u^*}{\partial y^{*2}} \tag{24}$$

$$Re_L \left(u^* \frac{\partial v^*}{\partial x^*} + v^* \frac{\partial v^*}{\partial y^*} \right) = -\frac{\partial p^*}{\partial y^*} + \frac{\partial^2 v^*}{\partial x^{*2}} + \frac{\partial^2 v^*}{\partial y^{*2}} \tag{25}$$

$$u^* \frac{\partial T^*}{\partial x^*} + v^* \frac{\partial T^*}{\partial y^*} = \frac{1}{Re_L Pr} \left(\frac{\partial^2 T^*}{\partial x^{*2}} + \frac{\partial^2 T^*}{\partial y^{*2}} \right) \tag{26}$$

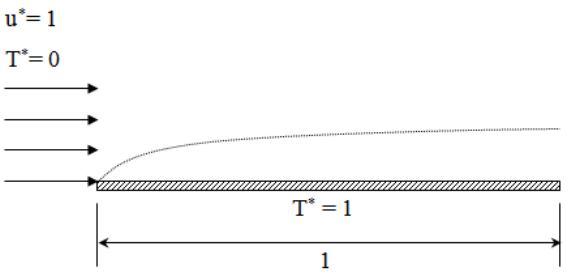

Figure 3: Non-dimensional problem setup for the flat plate.

where Re_L is the Reynolds number based on plate length, defined below.

$$Re_L = \frac{\rho U_\infty L}{\mu} \tag{27}$$

The non-dimensionalized plate gives the boundary conditions at the inlet and wall as well as the length of the domain. The velocity of the incoming stream, the length of the plate, and the temperature of the plate are set to unity. The temperature of the fluid stream is set to zero.

An examination of the dimensionless equations reveals that the fluid problem is dependent only upon the Reynolds number, and the thermal problem on a combination of the Reynolds and Prandtl numbers. A comparison between the dimensional and dimensionless forms of the governing equations shows that the Reynolds number corresponds to the density of the fluid, while the dynamic viscosity, free-stream velocity, and the plate length are all equal to unity. Therefore, the fluid problem can be fully manipulated by varying only the density of the fluid. The energy equation reveals that the product of the Reynolds and Prandtl numbers will scale inversely with the thermal diffusivity of the fluid. If the density, and therefore the Reynolds number, is considered fixed by the fluid problem, then the heat transfer problem may be fully manipulated by the Prandtl number. Since $Pr = \frac{\nu}{\alpha} = \frac{\mu c_p}{k}$, taking the heat capacity c_p to be equal to unity allows the heat transfer problem to be fully manipulated by varying only the thermal conductivity, k, of the fluid. Although the heat-transfer problem has some dependence on the Prandtl number, this simulation was run with a Prandtl number of 1.

Because full control over the numerical problem is afforded by varying only two parameters, this allows for easy input into the CFD program since, save for the density and thermal conductivity, all inputs, constants, and parameters will be equal to unity.

3.2 Numeric Setup

3.2.1 Mesh

An accurate CFD analysis requires a refined, high-quality mesh with ample error management. Since this analysis is concerned with the low Reynolds number portion of the boundary layer near the leading edge, a refined mesh was used toward the front of the plate, and a less refined mesh used toward the end of the plate. Since only the boundary-layer was of interest the mesh was more-refined close to the plate and less-refined far from the plate, as shown in Figure 4. This is referred to as a biased mesh, where the bias factor is defined as the ratio of the length of the first cell to the length of the last cell.

The boundary layer was resolved with a high number of grid points in order to increase the precision of the simulation in that region. Beginning at fifty grid points within the boundary layer defined by the 99.9% rule, the number of points were doubled with each iteration until the resolution in the boundary layer region reached 400 grid points. At this resolution the boundary layer was well-resolved, evidenced by the number of points in the temperature and velocity plots in Figures 5 through 7.

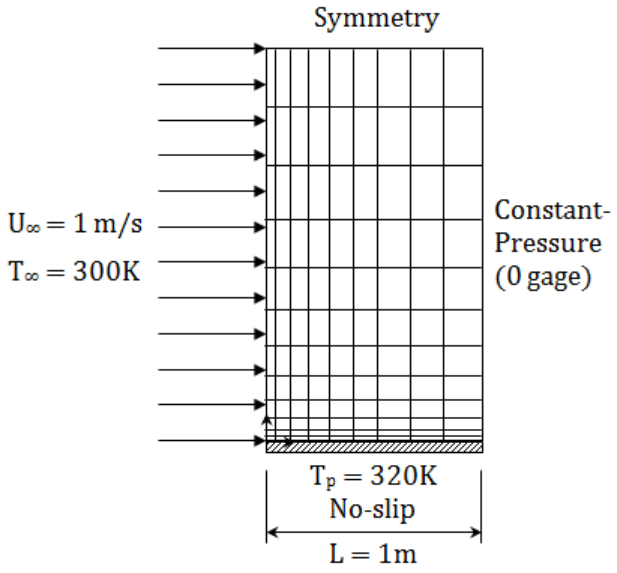

Figure 4: Flat plate domain showing refined mesh and boundary conditions

3.2.2 Boundary Conditions

One possible error source in the flat plate problem is that only the inlet and the surface of the plate have boundary conditions specified by the problem. Since the far-field and outlet don't have an imposed boundary condition, care must be made to ensure that the conditions used in these locations do not adversely affect

the numeric solution. This analysis used a symmetry condition at the far-field, and a constant-pressure condition at the outlet.

The symmetry condition forces the normal derivative to be zero at the surface at which the condition is applied. This translates to the conditions

$$\frac{d\vec{u}}{dy} = 0$$

and

$$\frac{dT}{dy} = 0,$$

both imposed at the top of the domain. If the height of the domain is not large enough then error from this boundary condition will propagate to the boundary layer and change the velocity and temperature field. This can be mitigated by increasing the domain height or by making the boundary layer thinner. Thinning the boundary layer would decrease the resolution of the solution near the leading edge, so the former method was used to reduce the error from the symmetry condition.

Another possible error source is the error associated with the constant-pressure condition at the outlet. This condition uses the static pressure specified at the outlet (in gage pressure) to extrapolate the other boundary conditions. The error associated with this condition is large when the flow is highly-viscous, and can be mitigated by increasing Re_L, the Reynolds number at the outlet. This introduces a trade-off between numerical error and solution precision, since increasing Re_L reduces the error from the constant-pressure condition at the cost of lower resolution at the tip.

The temperature conditions at the inlet and the plate are $T^* = 0$ and $T^* = 1$, respectively. Using these temperatures is not practical in FLUENT because the program has difficulty processing a temperature range of zero to one degrees Kelvin. Therefore, the plate temperature chosen was a more-reasonable 320 Kelvin, and the free-stream temperature 300 Kelvin.

3.3 Analytic and Numeric Comparison

Once the error mitigation from the boundary conditions and the mesh refinement is complete, the results of the simulation can be used to determine how well the analytic solution matches the numerical simulation. The following figures compare the results of the numeric solution with those of the analytic solutions to both the thermal and fluid boundary layers.

Figure 5 shows that the temperature profile given by the analytic solution to Equation 23 shows good agreement with the numeric solution obtained from CFD simulations. The analytic solution predicts the boundary layer profile better than the classic Pohlhausen solution, which has been included for comparative purposes. It is important to note that because the similarity variable, η, is defined differently for the leading-edge and classic solutions, a specified η in the leading-edge solution would not be consistent with the same η in the classical solution, hereafter defined as $\eta_B = y\sqrt{\frac{U_\infty}{\nu x}}$. Additionally, the Blasius boundary layer profile was plotted for comparison with the x-velocity in Figure 6, but was omitted from Figure 7 due to the low Reynolds number. The y-velocity profile derived in the Blasius solution varies inversely with $\mathrm{Re_x}$, since $v = \frac{U_\infty}{2\sqrt{Re_x}}\left(-f + \eta\frac{df}{d\eta}\right)$, so the low Reynolds number causes the Blasius y-velocity profile to be of a larger order of magnitude than the analytic and or numeric profiles, making it impractical to plot all three profiles on the same axes. This plot is included in Figure 12, located in Appendix A.

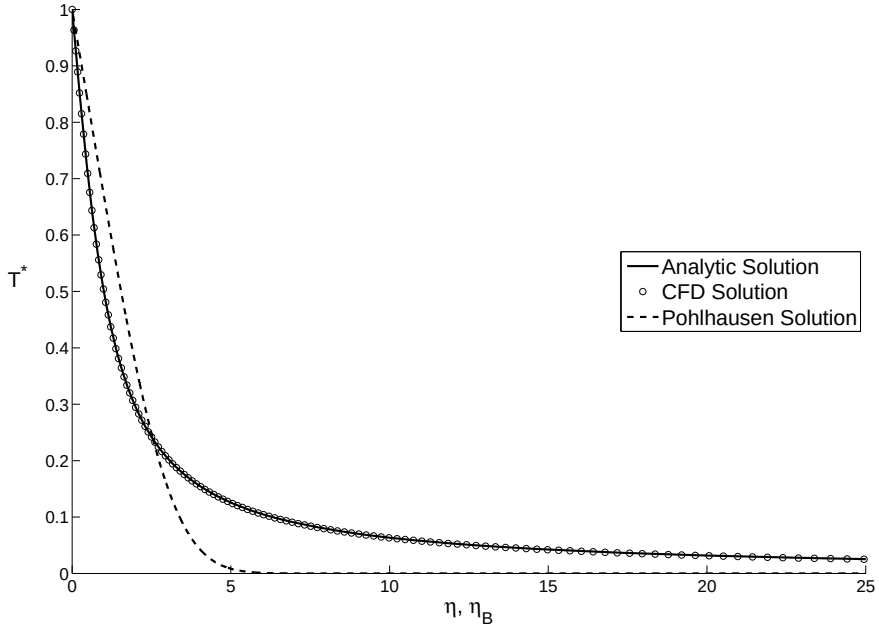

Figure 5: Analytic and numeric temperature profiles at the leading edge of the flat plate, $Re_x = 10^{-3}$.

Figures 6 and 7 compare the velocity profiles, reinforcing the agreement between the solutions when the Reynolds number is of order much less than one.

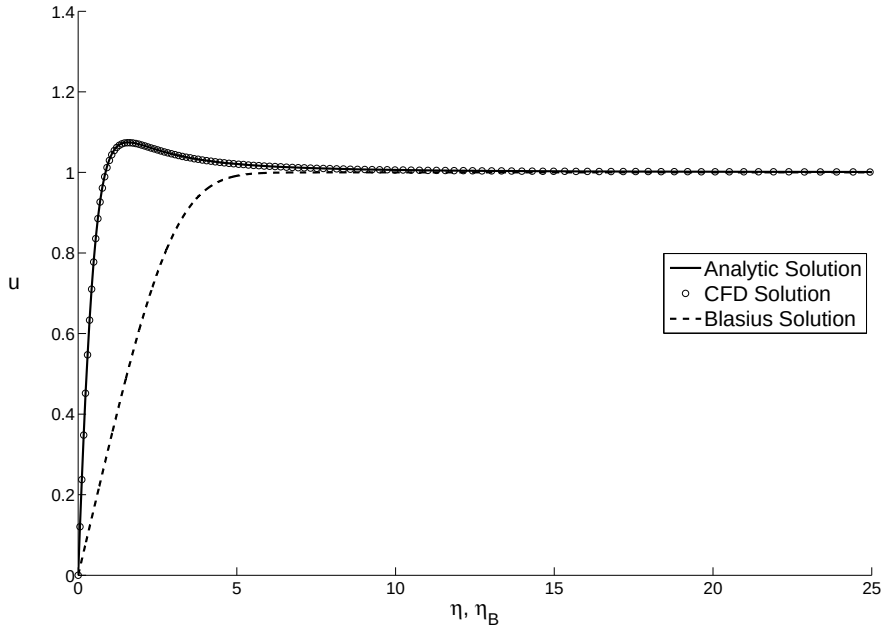

Figure 6: Analytic and numeric x-velocity profiles at the leading edge of the flat plate, $Re_x = 10^{-3}$.

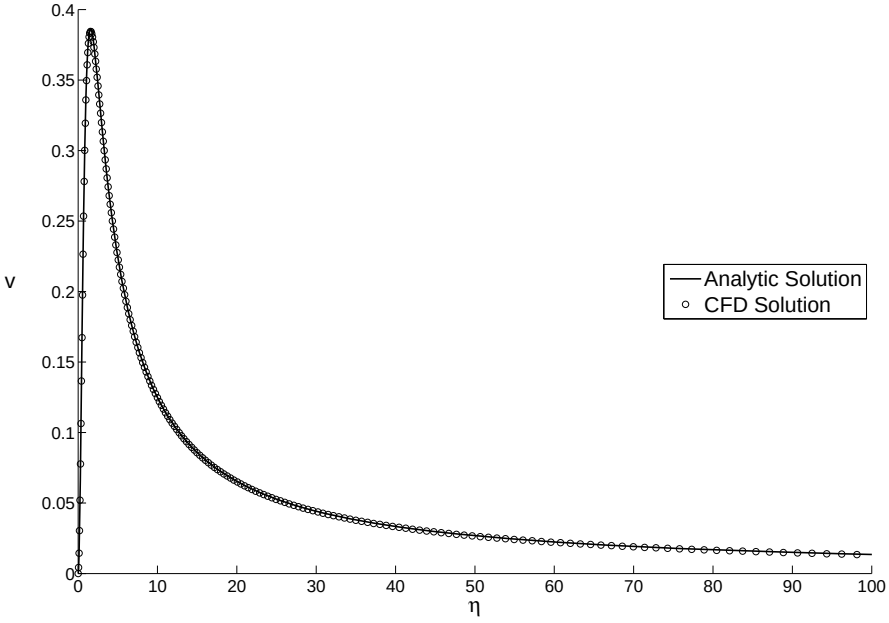

Figure 7: Analytic and numeric y-velocity profiles at the leading edge of the flat plate, $Re_x = 10^{-3}$.

Because the similarity scale is based on the leading-edge assumption that the Reynolds number is small, it is expected that the solution would become less accurate with increasing distance down the plate. Figure 8 plots the temperature profile versus η at increasing values of Re_x, and confirms that the analytic solution loses accuracy as the Reynolds number increases. The analytic solution provides good agreement up until $Re_x \approx 0.01$, but lacks good agreement when Re_x is of the order of unity or higher.

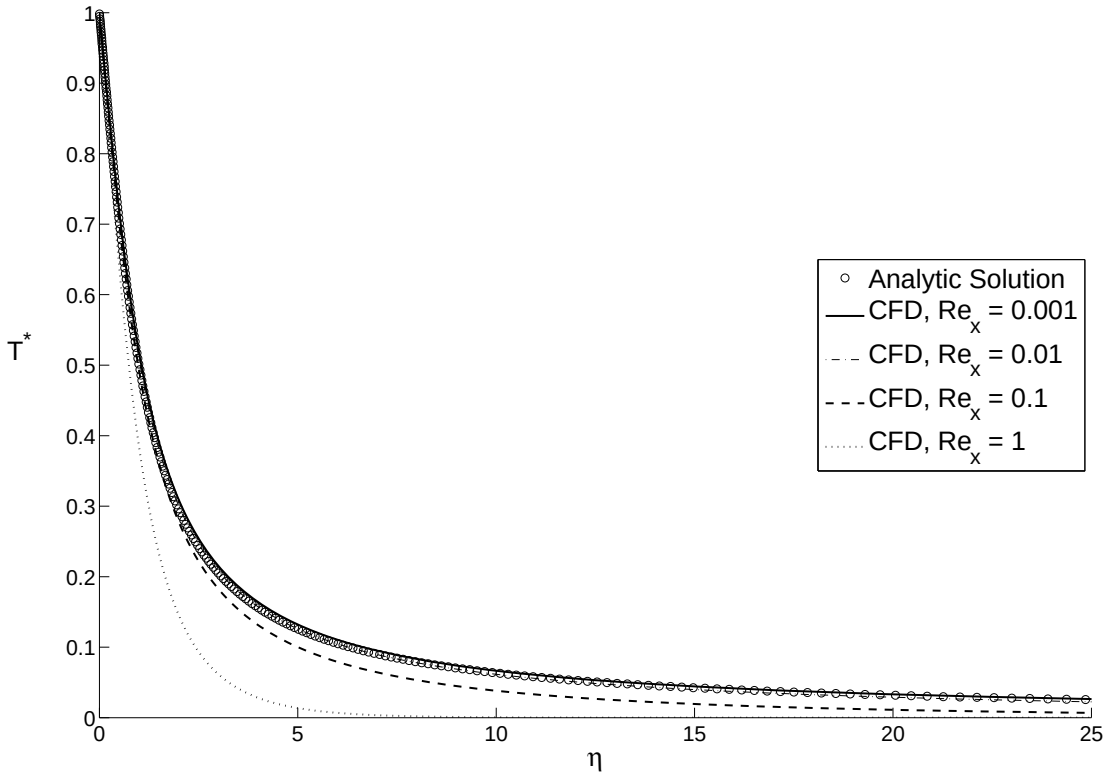

Figure 8: Analytic and numeric leading-order temperature profiles at the leading edge of the flat plate at various Reynolds numbers.

To verify that the restrictions on the thermal solution are identical to those on the fluid solution, Figures 9 and 10 plot the velocity profiles versus η at different values of Re_x ranging from 0.001 to unity, supporting the premise that the leading-edge solution loses accuracy as the Reynolds number increases.

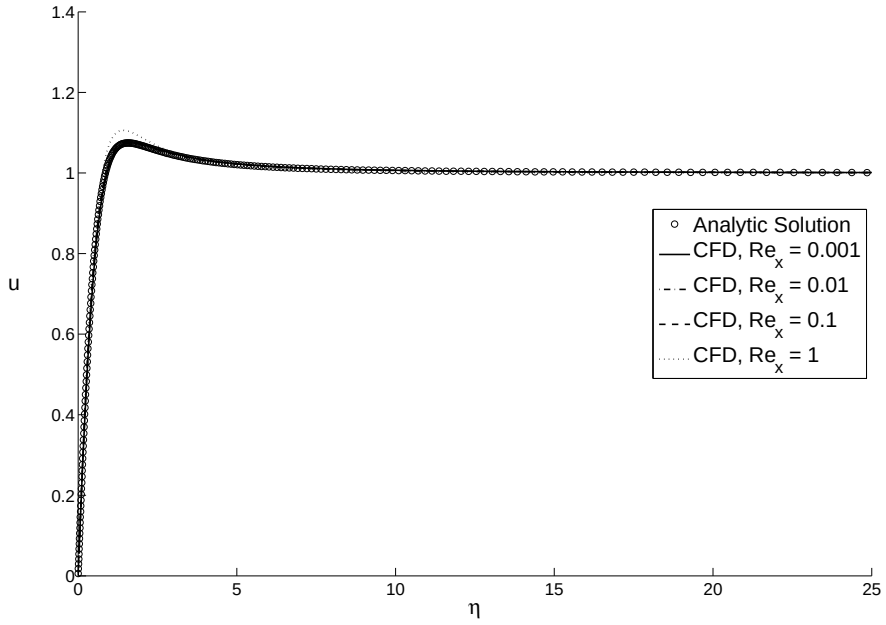

Figure 9: Analytic and numeric x-velocity profiles at the leading edge of the flat plate at various Reynolds numbers.

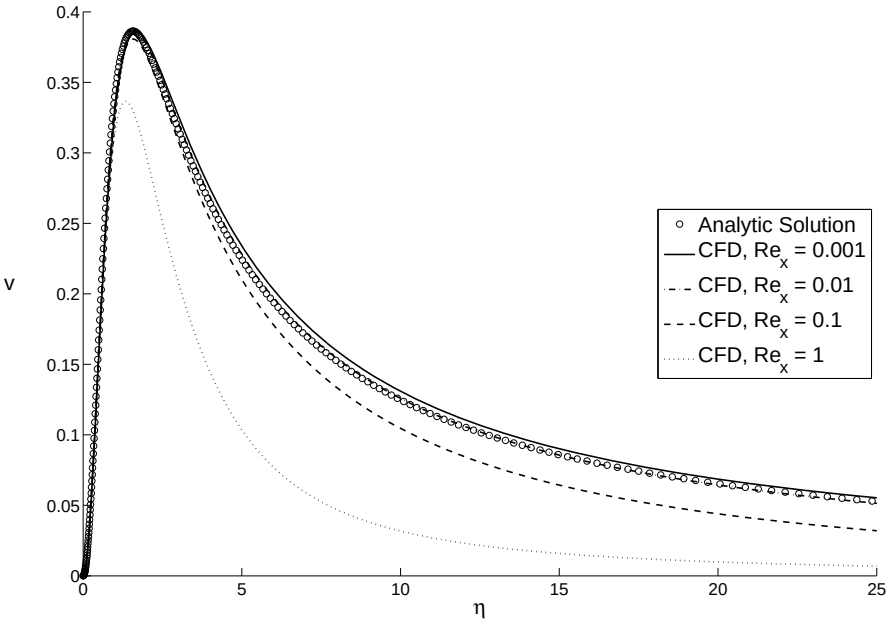

Figure 10: Analytic and numeric y-velocity profiles at the leading edge of the flat plate at various Reynolds numbers.

The effect of the Reynolds number on the solution accuracy can be seen in a plot of the difference between the analytic and CFD solutions, referred to hereafter as the absolute error, where the absolute error equals $T_{analytic} - T_{numeric}$. Figure 11 shows this error in the thermal boundary layer at different Reynolds numbers, and has been truncated at $\eta = 25$ in order to show the extrema located between $0 < \eta < 5$. Although perhaps not apparent below, each error term eventually decays to zero as $\eta \to \infty$.

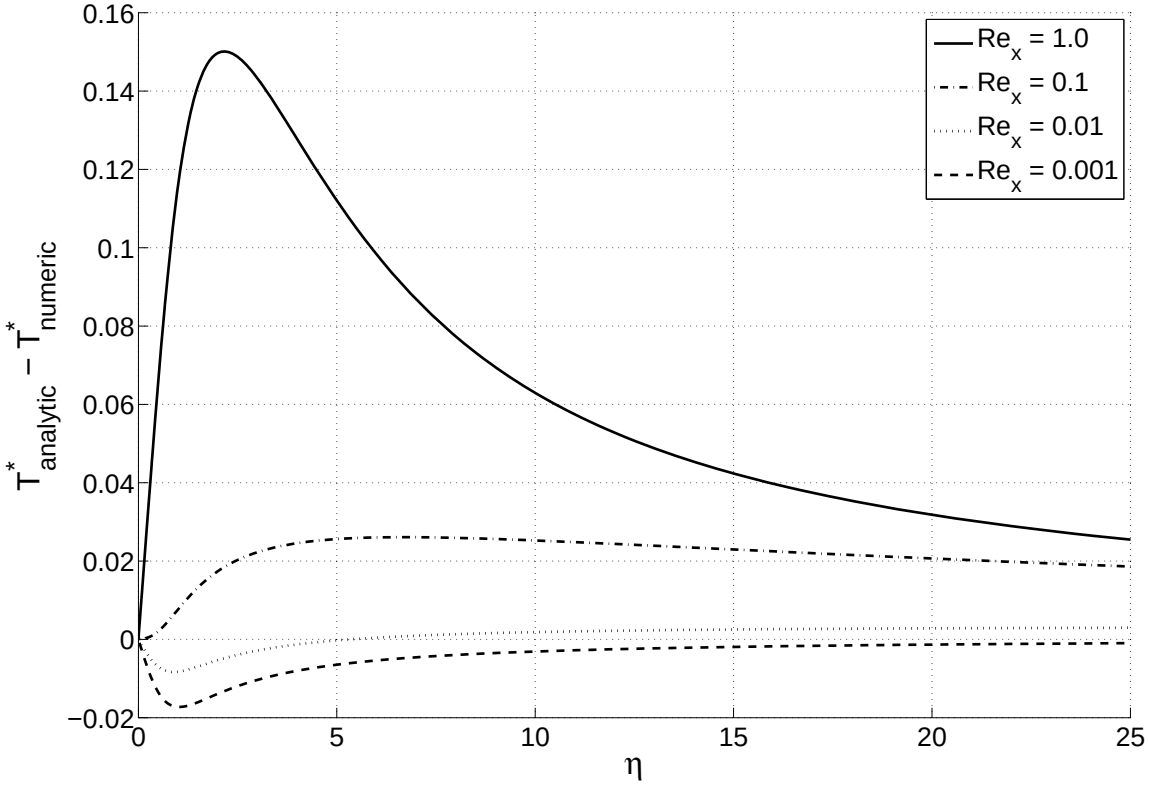

Figure 11: Difference between the analytic and CFD thermal boundary layer profiles, $0.001 \leq Re_x \leq 0.5$.

The decrease in accuracy of the analytic solution can be explained physically by considering the effects of convection. By taking the limit $Re_x \to 0$ the fluid effect is eliminated from Equation 15, resulting in a temperature solution that is decoupled from the fluid solution. While this is accurate when the Reynolds number is small, as Re_x increases convection becomes increasingly important, resulting in the analytic solution losing accuracy when convection is no longer negligible. Since this transition takes place rather quickly, the analytic solution is not accurate for Reynolds numbers larger than 0.1.

It is interesting to note that at values below $Re_x \approx 0.1$ the analytic solution initially undershoots the CFD solution. Examination of Equation 15 reveals that taking the limit $Re_x \to 0$ eliminates the convection term by eliminating the fluid effect, $f(\eta)$, from the energy equation. Taking this limit should result in the

analytic solution overshooting the numeric solution due to the thinning tendency of convection effects, but the local minima located at $\eta \approx 1$ indicates that at Reynolds numbers below approximately 0.1 this is not initially the case.

At higher Reynolds numbers the analytic solution predicts a boundary layer that is too large, confirming that the leading edge assumption becomes less accurate as distance down the plate increases.

4 Conclusion

The goal of this work was to develop a solution method that would allow for better representation of the thermal boundary layer over the flat plate. Since the classical flat plate boundary layer is only valid where the Reynolds number high, this work developed a solution valid at the leading edge. Even though the practical applications are somewhat limited, the solution process presented herein provides a useful method that could be used to develop similar solutions to other boundary layers.

The two-dimensional governing equations for the boundary layers of the flat plate were simplified and converted to the stream function. An order-of-magnitude analysis was performed using scales from these governing equations, and these scales used to convert the equations into similarity form. Once converted to similiarity form, the equations were simplified and the limit taken as $Re_x \to 0$.

A solution valid at the leading edge was developed for the thermal boundary layer, and the fluid boundary-layer solution was presented for the sake of completion. Once obtained, the analytic solutions were compared with a numeric solution obtained using computational fluid dynamics. The velocity and temperature profiles were compared first at low Reynolds numbers, then with increasing Reynolds number. These plots revealed that the analytic solution shows good agreement with the numeric up to Reynolds numbers of 0.01.

Recommendations for Future Work:

Since the analytic solution loses accuracy as the Reynolds number increases, the similarity functions $f(\eta)$ and $\hat{T}(\eta)$ should be written as functions of η and Re_x, such that $f = f(\eta, Re_x)$ and $\hat{T} = \hat{T}(\eta, Re_x)$. The appropriate derivatives would need to be substituted into Equations 7 and 8, and the resulting equation arranged by powers of Re_x. The leading-order terms should result in Equations 18 and 19, confirming the solutions presented herein.

A similar analysis could also be performed for the classic flat plate problem using the similarity scale developed by Blasius. Since the Blasius solution is not seen unless $Re_x > 10^5$, the similarity functions could also contain a Reynolds number dependence similar to that suggested above, where the leading-order solution should confirm the Blaisius and Pohlhausen solutions.

References

[1] Anderson, J. D., 2005, "Ludwig Prandtl's Boundary Layer," *Physics Today*, **58**, pp. 42-48.

[2] L. Prandtl, 1904, "Über Flüssigkeitsbewegung bei sehr kleiner Reibung," Verhandl III, Intern. Math Kongr., Heidelberg, Auch pp. 2-3.

[3] Munson, B. R., Young, D. F., and Okiishi, T. H., 2006, *Fundamentals of Fluid Mechanics*, 5th ed., John Wiley & Sons, Inc., Hoboken, NJ, pp. 293-294, Chap. 6.

[4] Blasius, H., 1908, "Grenzschichten in Flüssigkeiten mit kleiner Reibung," *Z. Math. Phys.,* **56**, pp. 1-57.

[5] Pohlhausen, E., 1921, "Der Wärmeaustausch zwischen festen Körpern und Flüssigkeiten mit kleiner Reibund und kleiner Wärmeleitung," *Z. angew. Math. Mech.*, **1**, pp. 115-121.

[6] Kundu, P.K., Cohen, I. M., and Dowling, D. R., 2012, *Fluid Mechanics*, 5th ed., Academic Press, Waltham, MA, pp. 369-380, Chap 9.

[7] Falker, V. W., and Skan, S. W., 1931, "Solutions of the boundary layer equations," *Phil. Mag.*, **12**, pp. 865-896.

[8] Thwaites, B., 1949, "Approximate calculation of the laminar boundary layer," *Aero. Quart*, **1**, 245-280.

[9] Ting, L., 1960, "Boundary Layer Over a Flat Plate in Presence of Shear Flow," *Phys. Fluids*, **3**, (1), pp. 78-81.

[10] Devan, L., 1965, "Approximate Solution of the Shear Flow Boundary Layer on a Flat Plate," *Phys. Fluids*, **8**, (12), pp. 2211-2215.

[11] Wediman, P.D., 1997, "Blasius Boundary Layer Flow Over an Irregular Leading Edge," *Phys. Fluids*, **9**, (5), pp. 1470-1472.

Appendices

Appendix A: Additional Figures

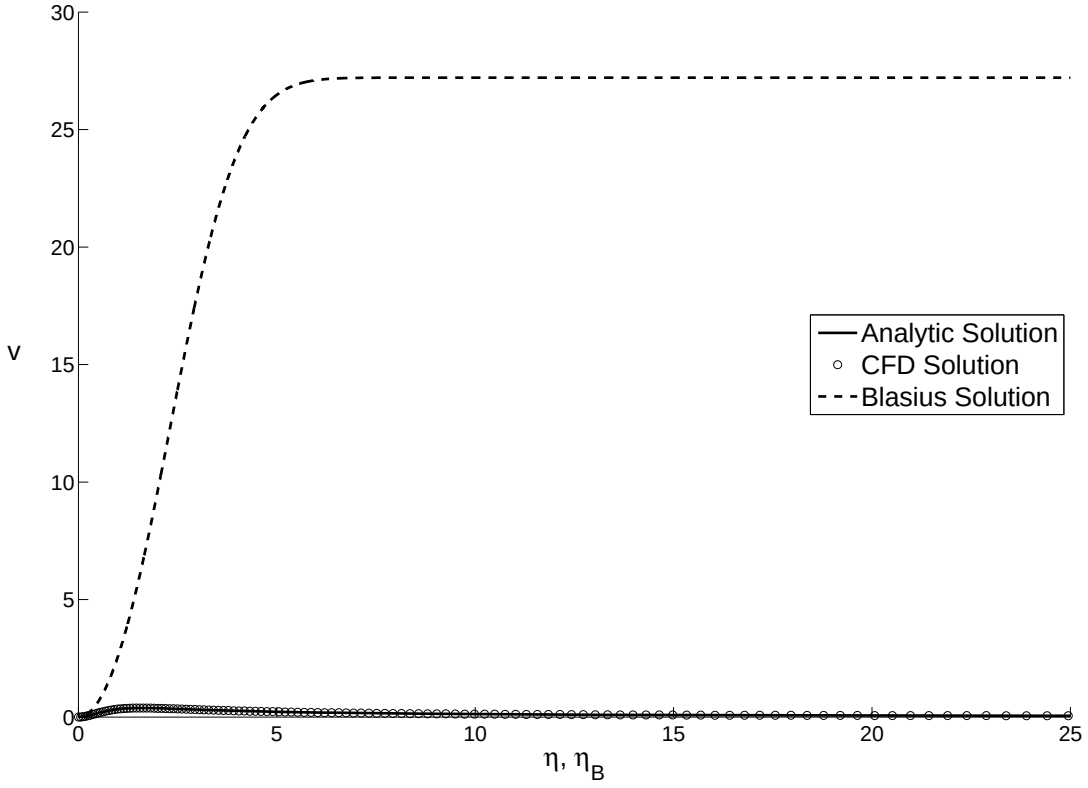

Figure 12: Y-Velocity Profile with Blasius Solution

Appendix B: MATLAB Code

```
% Thesis Research
% Author: Robert L Jessee

% This code solves the leading edge of the laminar flat plate boundary
% layer fluid and thermal profiles. It generates the analytic solution
% derived by Robert Jessee and Sai Rao, then takes CFD data from FLUENT and
% compares the analytic solution with that of the CFD simulation

clear;
clc;

% Load the CFD data for the entire field (data exported from FLUENT)
load FlatPlate_1x3_200x600_ReL100_BF10e5_Sorted.mat
set(0,'DefaultFigureWindowStyle','docked')    % Defaults figures to docked

%% CFD PARAMETERS AND FLOW SETUP

% Domain Size: 1m x 3m (Length x Height)
% Mesh Size: 200 elements by 600 elements (Length x Height)
% Bias Factor: 1 x 10^5
% T_infinity = 300 K
% T_plate = 320 K
% Note: These temperatures were chosen because FLUENT can't operate
% using a dimensionless temperature range of 0K to 1K, so the values of
% 320K and 300K were chosen arbitrarily, since reference properties were
% evaluated at 300K

%%%%%%%%%%%%%%%%%%%%%%%%%%%%%%%%%%%%%%%%%%%%%%%%%%%%%%%%%%%%%%%%%%%%%%%%%%%
% CFD DATA & VARIABLES
%%%%%%%%%%%%%%%%%%%%%%%%%%%%%%%%%%%%%%%%%%%%%%%%%%%%%%%%%%%%%%%%%%%%%%%%%%%
% The following section takes the velocity and temperature data from FLUENT
% and puts it in a form that makes it easier to compare with the numerical
% solution obtained from MATLAB

% Flow Parameters:
rho = 100;      % Density, [kg/m^3]
L = 1.0;        % Plate length, [m]
mu = 1.0;       % Dynamic viscosity, [kg/m-s]
U = 1.0;        % Free-stream velocity, [m/s]
alpha = .01;
nu = mu/rho;    % Kinematic viscosity, m^2/s
t_inf = 300;    % Temperature of incoming flow, in K
t_p = 320;      % Temperature of plate, in K
Pr = nu/alpha;
% Note: From the above values we can deduce that Re_L = 100, Pr = 1
y_max = 3.0;    % The height of the mesh above the plate (per unit length)

% Set upper and lower limits on eta (for graphing purposes)
eta_min = 0;
eta_max = 25;
```

```
%% LIST OF VARIABLES
% This section describes the variables and data imported from the CFD
% program (FLUENT) at the beginning of this code.

%%%%%%%%%%%%%%%%%%%%%%%%%%%%%%%%%%%%%%%%%%%%%%%%%%%%
% VARIABLES FROM THE SORTED CFD DATA
%%%%%%%%%%%%%%%%%%%%%%%%%%%%%%%%%%%%%%%%%%%%%%%%%%%%

% # y_nodes = 600;
% # x_nodes = 200;

%%%%%%% CELL CENTER VALUES %%%%%%%
% General solution data (taken at cell centers):
% x_fluent          x-location matrix
% y_fluent          y-location matrix
% u_fluent          x-velocity matrix
% v_fluent          y-velocity matrix
% t_fluent          temperature matrix
% eta_fluent        similarity variable matrix, where eta = y/x

% Generate a matrix for the dimensionless temperature, T^*, based on
% cell-center values
tstar_fluent = (t_fluent - t_inf)./(t_p - t_inf);

% Generate a matrix for the Reynolds number in the CFD data based on
% cell-center values
Rex_f = (U*x_fluent(1,:))./nu;

%%%%%%% NAMED LOCATION VALUES %%%%%%%

% Data Locations:
% x(1) = 0.000001
% x(2) = 0.000005
% x(3) = 0.0000075
% x(4) = 0.00001
% x(5) = 0.000025
% x(6) = 0.00005
% x(7) = 0.000075
% x(8) = 0.0001
% x(9) = 0.00025
% x(10) = 0.0005
% x(11) = 0.00075
% x(12) = 0.001
% x(13) = 0.0025
% x(14) = 0.005
% x(15) = 0.0075
% x(16) = 0.01
% x(17) = 0.025
% x(18) = 0.05
% x(19) = 0.1

% 'Named Locations' (places where x-value is specified and interpolated for
% fixed Re_x
% x_f_nl         x-location array (600x10)
% y_f_nl         y-location array (602x1)
% u_f_nl         x-velocity array (602x10)
```

```
% v_f_nl         x-velocity array (602x6), data only taken from P1 to P6
% tstar_f_nl     temperature array (602x6), data only taken from P1 to P6
% eta_f_nl       similarity variable array (602x10)
% eta_blas_nl = y_f_nl./sqrt(x_f_nl );

% Generate a matrix for the dimensionless temperature, T^*, based on
% named-location values
tstar_NL = (t_NL - t_inf)./(t_p - t_inf);

% Generate a matrix for the Reynolds number in the CFD data based on
% named-location values
Rex_NL = (U.*x_NL)/nu;

eta_blas_nl = zeros(length(y_NL),length(x_NL));
for i = 1:length(x_NL) - 1
    eta_blas_nl(:,i) = y_NL(:)./sqrt(x_NL(i));
end

%% BLASIUS CLASSICAL SOLUTION

% Fluid boundary conditions
f0_0 = 0;               % f0(0)
g0_0 = 0;               % f0'(0)
h0_0 = 0.33205;         % f0''(0); this is the shooting term for the
                        % Blasius (leading-order) solution. Solved value is
                        % f0''(0) = 0.33205
% Thermal boundary conditions
r0_0 = 0;                       % T(0)
s0_0 = 0.33205.*(Pr.^(1/3));       % T'(0)

eta_start = eta_min;
eta_end = eta_max;
d_eta = 0.001;
nsteps = (eta_end - eta_start)/d_eta;
etaspan = linspace(eta_start, eta_end, nsteps);
options = odeset('RelTol',0.00001,'Stats','on');

% Solve the leading-order equation for f0(eta,R)
% f0(1) = f0        % f0(2) = f0'       % f0(3) = f0''
[eta0,f0] = ode45(@BlasPohl,etaspan,[f0_0 g0_0 h0_0 r0_0 s0_0], options);

u_blas = f0(:,2);

% v_blas = zeros(length(eta0),length(Rex_f));
% for i = 1:length(Rex_f)
% %     v_blas(:,i) = (U./sqrt(Rex_f(1,i))).*(eta0.*f0(:,2) - f0(:,1));
%     v_blas(:,i) = (eta0.*f0(:,2) - f0(:,1));
% end
v_blas = (eta0.*f0(:,2) - f0(:,1));
t_blas = 1 - f0(:,4);

%% ANALYTIC SOLUTION
% This portion of the code calculates the analytic fluid and thermal
% solutions at the flat plate's leading edge based on the similarity values
% at both the cell-center and named locations
```

```
%%%%%%%%%%%%%% FLUID SOLUTION %%%%%%%%%%%%%%

%%% CELL CENTERS %%%
% Analytic fluid profile & derivative at cell centers
f0_fluent = (4/(pi^2 - 4))*((pi/2.*eta_fluent).*atan(eta_fluent) - eta_fluent);
df0_fluent = (4./((pi^2 - 4).*(1+eta_fluent.^2))).*(eta_fluent.*(pi/2-eta_fluent) +↙
(pi/2).*(1+eta_fluent.^2).*atan(eta_fluent));

%%% NAMED LOCATIONS %%%
% Analytic fluid profile & derivative at named locations
f0_NL = (4/(pi^2 - 4))*((pi/2.*eta_NL).*atan(eta_NL) - eta_NL);
df0_NL = (4./((pi^2 - 4).*(1+eta_NL.^2))).*(eta_NL.*(pi/2-eta_NL) + (pi/2).*(1+eta_NL.↙
^2).*atan(eta_NL));

u0_fluent = df0_fluent;
v0_fluent = (-4./((pi^2 - 4).*(1+eta_fluent.^2))).*((1+eta_fluent.^2).*atan(eta_fluent) -↙
eta_fluent.*(1+(pi/2).*eta_fluent));

u0_NL = df0_NL;
v0_NL = (-4./((pi^2 - 4).*(1+eta_NL.^2))).*((1+eta_NL.^2).*atan(eta_NL) - eta_NL.*(1+↙
(pi/2).*eta_NL));
% v0_NL = zeros(size(f0_NL));
% for i = 1:min(size((v_NL)))
%     v0_NL(:,i) = f0_NL(:,i) - eta_NL(:,i).*df0_NL(:,i);
% end

%%%%%%%%%%%%%% THERMAL SOLUTION %%%%%%%%%%%%%%

%%% CELL CENTERS %%%
% Analytic dimensionless temperature profile at cell centers
t0_fluent = 1 - (2/pi).*atan(eta_fluent);

%%% NAMED LOCATIONS %%%
% Analytic dimensionless temperature profile at named locations
t0_NL = 1 - (2/pi).*atan(eta_NL);

%% COMPARATIVE ANALYSIS
% This section compares the analytic and numeric solutions to see how
% accurate the analytic predictions are

%%%%% PLOTS AT REYNOLDS NUMBERS = 1x10^-3 %%%%%

%%%%% Plot the x-velocity for comparison %%%%%
lw = 2;
figure(1)
clf
hold on
P = 2;
% Analytic Solution
plot(eta_NL(:,P),u0_NL(:,P),'-k','linewidth', lw)
% CFD Solution
plot(eta_NL(:,P),u_NL(:,P),'ok','markers',6)
% Blasius Solution
plot(eta0,u_blas,'--k','linewidth', lw)
xlim([eta_min eta_max])
xlab_1 = xlabel('\eta, \eta_B','fontsize', 20);
```

```
ylab_1 = ylabel('u','fontsize', 20);
set(gca,'FontSize',16)
set(get(gca,'YLabel'),'Rotation',0.0)
set(ylab_1,'Position',get(ylab_1,'Position') - [1 0 0])
tit_1 = title(['X-Velocity Profile Re_x = ' num2str(Rex_NL(1,P)) ', Leading-Order↙
Solution'],'fontsize', 20);
leg1 = legend('Analytic Solution','CFD Solution','Blasius Solution','Location','east');
set(leg1,'fontsize',20)

%%%%% Plot the y-velocity for comparison %%%%%
figure(2)
clf
hold on
P = 2;
% Analytic Solution
plot(eta_NL(:,P),v0_NL(:,P),'-k','linewidth', lw)
% CFD Solution
plot(eta_NL(:,P),v_NL(:,P),'ok','markers',6)
% Blasius Solution
% plot(eta0,1./(2*sqrt(Rex_NL(1,P))).*v_blas,'--k','linewidth', lw)
xlim([eta_min eta_max])
% ylim([0 1])
xlab_2 = xlabel('\eta','fontsize', 20);
ylab_2 = ylabel('v','fontsize', 20);
set(ylab_2,'Position',get(ylab_2,'Position') - [1 0 0])
set(gca,'FontSize',16)
set(get(gca,'YLabel'),'Rotation',0.0)
tit_2 = title(['Y-Velocity Profile Re_x = ' num2str(Rex_NL(1,P)) ', Leading-Order↙
Solution'],'fontsize', 20);
leg2 = legend('Analytic Solution','CFD Solution','Blasius Solution','Location','east');
set(leg2,'fontsize',20)

%%%%% Plot the temperature profile for comparison %%%%%
figure(3)
clf
hold on
P = 2;
% Analytic Solution
plot(eta_NL(:,P),t0_NL(:,P),'-k','linewidth', lw)
% CFD Solution
plot(eta_NL(:,P),tstar_NL(:,P),'ok','markers',6)
% Pohlhausen Solution
plot(eta0,t_blas,'--k','linewidth', lw)
xlim([eta_min eta_max])
xlab_3 = xlabel('\eta, \eta_B','fontsize', 20);
ylab_3 = ylabel('T^*','fontsize', 20);
set(ylab_3,'Position',get(ylab_3,'Position') - [1 0 0])
set(gca,'FontSize',16)
set(get(gca,'YLabel'),'Rotation',0.0)
tit_3 = title(['Temperature Profile Re_x = ' num2str(Rex_NL(1,P)) ', Leading-Order↙
Solution'],'fontsize', 20);
leg3 = legend('Analytic Solution','CFD Solution','Pohlhausen↙
Solution','Location','east');
set(leg3,'fontsize',20)
%
```

```
%%

%%%%% PLOTS AT VARIOUS REYNOLDS NUMBERS %%%%%

% PLOTS AT NAMED LOCATIONS
%%%%% Plot the x-velocity at Re_x = 0.001, 0.01, 0.1, and 1 %%%%%

% x1 = 2;          % Re_x = 0.001
% x2 = 3;          % Re_x = 0.01
% x3 = 4;          % Re_x = 0.1
% x4 = 5;          % Re_x = 1
% x5 = 6;          % Re_x = 0.001

x1 = 26;
x2 = 86;
% x3 = 114;  Re_x = 0.025
x3 = 162;
x4 = 242;
% x5 = 194;
% x6 = 218;

figure(4)
clf
hold on
% Analytic Solution
plot(eta_fluent(:,x2),u0_fluent(:,x2),'-b','linewidth',lw)
% CFD Solution at varying Re_x
plot(eta_fluent(:,x1),u_fluent(:,x1),'-r','linewidth',lw)
plot(eta_fluent(:,x2),u_fluent(:,x2),'-k','linewidth',lw)
plot(eta_fluent(:,x3),u_fluent(:,x3),'--k','linewidth',lw)
plot(eta_fluent(:,x4),u_fluent(:,x4),':k','linewidth',lw)
xlim([eta_min eta_max])
xlab_4 = xlabel('\eta','fontsize', 20);
ylab_4 = ylabel('u','fontsize', 20);
set(gca,'FontSize',16)
set(get(gca,'YLabel'),'Rotation',0.0)
set(ylab_4,'Position',get(ylab_4,'Position') - [1 0 0])
tit_4 = title('X-Velocity Profile at Different Re_x Values, Leading-Order↙
Solution','fontsize', 20);
leg4 = legend('Analytic Solution',['CFD, Re_x = ' num2str(Rex_f(1,x1),'%0.3f') ],['CFD,↙
Re_x = ' num2str(Rex_f(1,x2),'%0.2f') ],['CFD, Re_x = ' num2str(Rex_f(1,x3),'%0.1f') ],↙
['CFD, Re_x = ' num2str(Rex_f(1,x4),'%0.0f') ],'Location','east');
set(leg4,'fontsize',20)

% %%%%% Plot the y-velocity at Re_x = 0.001, 0.01, 0.1, and 1 %%%%%
figure(5)
clf
hold on
% Analytic Solution
plot(eta_fluent(:,x2),v0_fluent(:,x2),'-b','linewidth',lw)
% CFD Solution at varying Re_x
plot(eta_fluent(:,x1),v_fluent(:,x1),'-r','linewidth',lw)
plot(eta_fluent(:,x2),v_fluent(:,x2),'-k','linewidth',lw)
plot(eta_fluent(:,x3),v_fluent(:,x3),'--k','linewidth',lw)
plot(eta_fluent(:,x4),v_fluent(:,x4),':k','linewidth',2)
xlim([eta_min eta_max])
```

```
xlab_5 = xlabel('\eta','fontsize', 20);
ylab_5 = ylabel('v','fontsize', 20);
set(gca,'FontSize',16)
set(get(gca,'YLabel'),'Rotation',0.0)
set(ylab_5,'Position',get(ylab_5,'Position') - [1 0 0])
tit_5 = title('Y-Velocity Profile at Different Re_x Values, Leading-Order↙
Solution','fontsize', 20);
leg5 = legend('Analytic Solution',['CFD, Re_x = ' num2str(Rex_f(1,x1),'%0.3f') ],['CFD,↙
Re_x = ' num2str(Rex_f(1,x2),'%0.2f') ],['CFD, Re_x = ' num2str(Rex_f(1,x3),'%0.1f') ],↙
['CFD, Re_x = ' num2str(Rex_f(1,x4),'%0.0f') ],'Location','east');
set(leg5,'fontsize',20)

% %%%%% Plot the temperature profile at Re_x = 0.001, 0.01, 0.1, and 1 %%%%%
figure(6)
clf
hold on
% Analytic Solution
plot(eta_fluent(:,x2),t0_fluent(:,x2),'-b','linewidth',lw)
% CFD Solution at varying Re_x
plot(eta_fluent(:,x1),tstar_fluent(:,x1),'-r','linewidth',lw)
plot(eta_fluent(:,x2),tstar_fluent(:,x2),'-k')
plot(eta_fluent(:,x3),tstar_fluent(:,x3),'--k','linewidth',lw)
plot(eta_fluent(:,x4),tstar_fluent(:,x4),':k','linewidth',lw)
xlim([eta_min eta_max])
xlab_6 = xlabel('\eta','fontsize', 20);
ylab_6 = ylabel('T^*','fontsize', 20);
set(gca,'FontSize',16)
set(get(gca,'YLabel'),'Rotation',0.0)
set(ylab_6,'Position',get(ylab_6,'Position') - [1 0 0])
tit_6 = title('Temperature Profile at Different Re_x Values, Leading-Order↙
Solution','fontsize', 20);
leg6 = legend('Analytic Solution',['CFD, Re_x = ' num2str(Rex_f(1,x1),'%0.3f') ],['CFD,↙
Re_x = ' num2str(Rex_f(1,x2),'%0.2f') ],['CFD, Re_x = ' num2str(Rex_f(1,x3),'%0.1f') ],↙
['CFD, Re_x = ' num2str(Rex_f(1,x4),'%0.0f') ],'Location','east');
set(leg6,'fontsize',20)

%% ERROR ANALYSIS

%%%%% ABSOLUTE DIFFERENCE %%%%%

% Calculate the absolute difference between the analytic and CFD solutions
% at each cell center
diff_u = zeros(size(u0_fluent));
diff_v = diff_u;
diff_tstar = diff_u;
for i = 1:min(size(u0_fluent))
    diff_u(:,i) = u0_fluent(:,i) - u_fluent(:,i);
    diff_v(:,i) = v0_fluent(:,i) - v_fluent(:,i);
    diff_tstar(:,i) = t0_fluent(:,i) - tstar_fluent(:,i);
end

% Calculate the absolute difference between the analytic and CFD solutions
% at each named location

diff_u_NL = u0_NL - u_NL;
diff_v_NL = zeros(size(v_NL));
```

```
diff_tstar_NL = zeros(size(v_NL));
for i = 1:6
    diff_v_NL(:,i) = v0_NL(:,i) - v_NL(:,i);
    diff_tstar_NL(:,i) = t0_NL(:,i) - tstar_NL(:,i);
end

%%%%% PLOT THE DIFFERENCE BETWEEN THE ANALYTIC AND CFD %%%%%
% x = 26;       Re_x  = 0.0011
% x = 86;       Re_x  = 0.010
% x = 114;      Re_x  = 0.025
% x = 138;      Re_x  = 0.050
% x = 162;      Re_x  = 0.101
% x = 194;      Re_x  = 0.257
% x = 216;      Re_x  = 0.487
% x = 218;      Re_x  = 0.516
% x = 242       Re_x  = 1
% x = 298       Re_x  = 5
% x = 352       Re_x  = 25

x1 = 26;
x2 = 26;
x3 = 86;
x4 = 162;
x5 = 242;

lw = 2;     % Set the weight of the lines to be plotted

figure(7)
clf
hold on
plot(eta_fluent(:,x5),diff_tstar(:,x5),'-k','linewidth',lw)
plot(eta_fluent(:,x4),diff_tstar(:,x4),'-.k','linewidth',lw)
plot(eta_fluent(:,x3),diff_tstar(:,x3),':k','linewidth',lw)
plot(eta_fluent(:,x2),diff_tstar(:,x2),'--k','linewidth',lw)
% plot(eta_fluent(:,x1),diff_tstar(:,x1),'-k','linewidth',lw)
% plot(eta_fluent(:,x6),diff_tstar(:,x6),'--k','linewidth',lw)
xlim([eta_min eta_max])
% ylim([-0.02 0.1])
xlab_9 = xlabel('\eta','fontsize', 24);
ylab_9 = ylabel('T^*_{analytic} - T^*_{numeric}','fontsize', 24);
set(gca,'FontSize',20)
% tit_9 = title('Temperature Difference at Different Re_x Values, Leading-Order↙
Solution','fontsize', 24);
leg9 = legend(['Re_x = ' num2str(Rex_f(1,x5),'%0.1f') ], ['Re_x = ' num2str(Rex_f(1,↙
x4),'%0.1f') ], ['Re_x = ' num2str(Rex_f(1,x3),'%0.2f') ], ['Re_x = ' num2str(Rex_f(1,↙
x2),'%0.3f') ],'Location','northeast');

%%%%% Plot the y-velocity for comparison, include classic solution %%%%%
figure(8)
clf
hold on
P = 2;
% Analytic Solution
plot(eta_NL(:,P),v0_NL(:,P),'-k','linewidth', lw)
% CFD Solution
plot(eta_NL(:,P),v_NL(:,P),'ok','markers',6)
```

```
% Blasius Solution
plot(eta0,1./(2*sqrt(Rex_NL(1,P))).*v_blas,'--k','linewidth', lw)
xlim([eta_min 25])
% ylim([0 1])
xlab_2 = xlabel('\eta, \eta_B','fontsize', 20);
ylab_2 = ylabel('v','fontsize', 20);
set(ylab_2,'Position',get(ylab_2,'Position') - [1 0 0])
set(gca,'FontSize',16)
set(get(gca,'YLabel'),'Rotation',0.0)
tit_2 = title(['Y-Velocity Profile Re_x = ' num2str(Rex_NL(1,P)) ', Leading-Order↙
Solution'],'fontsize', 20);
leg2 = legend('Analytic Solution','CFD Solution','Blasius Solution','Location','east');
set(leg2,'fontsize',20)
```

Vita

Robert Lawrence Jessee is a native of South Carolina, and recieved his bachelor's degree in Mechanical Engineering from Clemson University in 2008. He taught high school math and science at Chalmette High School in Chalmette, Louisiana for 5 years after graduating from Clemson, and decided to work towards an advanced engineering degree after his interest in teaching waned. He enrolled at Louisiana State University in the fall semester of 2013, and plans to work as a mechanical engineer after graduation.